JOURNAL OF GEOPHYSICAL RESEARCH, VOL. 104, NO. E4, PAGES 8781–8794, APRIL 25, 1999

The color of Mars: Spectrophotometric measurements at the Pathfinder landing site

J. N. Maki and J. J. Lorre
Jet Propulsion Laboratory, California Institute of Technology, Pasadena

P. H. Smith
Lunar and Planetary Laboratory, University of Arizona, Tucson

R. D. Brandt and D. J. Steinwand
Jet Propulsion Laboratory, Pasadena, California

Abstract. We calculate the color of the Martian sky and surface directly using the absolute calibration of the Mars Pathfinder (MPF) lander camera, which was observed to be stable during the mission. The measured colors of the Martian sky and surface at the Pathfinder site are identical to the Viking sites, i.e., a predominantly yellowish brown color with only subtle variations. These colors are distributed continuously and fall into five overlapping groups with distinct average colors and unique spatial characteristics: shadowed soil, soil, soil/rock mixtures, rock, and sky. We report that the primary difference between the sky color and the color of the rocks is due to a difference in brightness. Measurements of the sky color show that the sky reddens away from the Sun and toward the horizon and that the sky color varies with time of day and is reddest at local noon. We present a true color picture of the Martian surface and color enhancement techniques that increase image saturation, maximize color discriminability while preserving hue, and eliminate brightness variations while preserving the chromaticity of the scene. Although Mars has long been called the "red" planet, quantitative measurements of the surface color from telescopic and surface observations indicate a light to moderate yellowish brown color. The Pathfinder camera measurements presented here support the claim that the red planet is not red but indeed yellowish brown.

1. Introduction

In this paper we present spectral radiance and color measurements of the Martian sky and surface from data acquired by the Mars Pathfinder (MPF) lander camera. We calculate the perceptual color (Commission Internationale de l'Eclairage (CIE) tristimulus values) of the Martian sky and surface directly using the absolute radiometric calibration of the camera. This differs from the approach used by *Huck et al.* [1977] on the Viking lander, where the spectral radiance was estimated using a linear combination of basis functions [*Park and Huck*, 1976]. The Viking method was necessitated by the fact that the Viking color filters had significant out-of-band response and were performance-limited by planetary contamination requirements and corresponding biocleaning techniques. Our method eliminates the need for separate knowledge of the solar irradiance, the spectral reflectance of the scene, and the color calibration chips on the lander. We note here that color chips alone cannot be used for absolute color calibration because the colors of the chips are dependent on the illumination conditions (direct sunlight, atmospheric scattered light, and light reflected off of the lander) under which they are viewed. By using the absolute calibration of the camera, we eliminate the need for separate knowledge of the illumination of the scene; this also allows us to examine the change in the color of the sky and surface as a function of time of day.

Paper number 98JE01767.
0148-0227/99/98JE-01767$09.00

Color is that aspect of visual perception by which an observer may distinguish differences between two structure-free fields of view of the same size and shape caused by differences in the spectral composition of the radiant energy [*Wyszecki and Stiles*, 1982]. The human visual system compares the integrated intensity over three spectral regions (red, green, and blue) and classifies these intensities into the thousands of discernible colors that make up color vision. Humans rely on this experience in recognizing colors to assist in classifying objects and scenes. The calculation of the perceptual color of Mars allows an individual to experience the same visual sensation (aside from color acclimation) as if the individual were actually on the Martian surface. The calculation of the color of the Pathfinder landing site also enables the opportunity to directly compare the color of the Pathfinder landing site to the reported Viking colors. For these reasons, the calculation and the reproduction of the true color of the Martian surface is a useful and significant analysis tool both for the layman and for the experienced specialist.

The process of measuring and displaying the color of an object or scene consists of three steps: measuring the spectral radiance of the scene or object, converting the spectral radiance into colorimetric units, and converting the resulting colorimetric units into pixel intensity values for a particular display device. We discuss each of these operations in order.

Table 1. Responsivity Parameters for the Pathfinder Camera

Filter	Wavelength λ, nm	Bandpass δλ, nm	R_0	R_1	R_2
R0	443.2	26.2	117.9	−0.392	−0.0006
R5	671.2	19.5	557.3	−0.575	−0.0014
R6	752.0	18.9	787.1	−0.247	−0.0019
R8	599.5	21.0	592.7	−0.598	−0.0013
R9	530.8	29.6	578.6	−0.893	−0.0021
R10	479.9	27.0	368.1	−0.668	−0.0019
R11	966.8	29.6	393.5	2.185	0.0065
L0	443.3	26.2	128.8	−0.387	−0.0007
L5	671.4	19.7	575.3	−0.570	−0.0013
L6	801.6	21.0	872.2	0.237	−0.0029
L7	858.4	34.4	1435	2.491	0.0035
L8	897.9	40.8	1120	3.006	0.0059
L9	931.1	27.0	478.7	1.926	0.0051
L10	1002.9	29.1	213.4	1.606	0.0052
L11	968.0	31.4	395.8	2.027	0.0051

See *Reid et al.* [this issue] for a more detailed discussion of camera calibration.

2. Spectral Radiance

When the Pathfinder lander camera images a scene on the Martian surface, the amount of signal measured by the camera is digitized (to 12 bits) and sent back to Earth. Dividing this digital number (DN) by the exposure time t yields a flux value proportional to the absolute radiance of the image scene. The ratio of the measured signal to the absolute radiance of the scene is the sensitivity or responsivity R of the instrument. The camera responsivity in units of (DN/s)/[W/(m^2 st μm)] is

$$R(\lambda) = A\Omega\delta\lambda T_{\text{filter}}(\lambda)\frac{\text{QE}(\lambda)}{\text{gain}}\frac{\lambda}{hc} \tag{1}$$

where A is the area of a detector pixel in units of square meters, Ω is the solid angle subtended by the aperture (at the pixel-aperture distance) in steradians, $\delta\lambda$ is the spectral bandpass of the system in microns, $T_{\text{filter}}(\lambda)$ is the transmission of the optics and bandpass filter, QE is the quantum efficiency of the CCD detector, gain is the number of electrons per DN, h is Planck's constant (6.626×10^{-34} J s), c is the speed of light (2.998×10^8 m/s), and λ is the photon wavelength in nanometers. The camera responsivity can be approximated by a quadratic function in temperature that takes the form

$$R(\lambda, T) = R_0(\lambda) + R_1(\lambda)T + R_2(\lambda)T^2 \tag{2}$$

where the temperature T is in degrees Celsius and the values for $R_0(\lambda)$, $R_1(\lambda)$, and $R_2(\lambda)$ are included in Table 1. The work presented here is based on the preflight calibration, which was observed to be stable throughout the landed mission. For a more detailed discussion of camera calibration, see *Reid et al.* [this issue].

The absolute radiance S of a single pixel (at a location i, j in an image) is given by

$$S(i, j) = \frac{\text{DN}(i, j)}{tR(\lambda, T)G(i, j)} \tag{3}$$

where DN(i, j) is the instrument signal (in units of DN), $G(i, j)$ is the normalized flat field of the camera system (which corrects for the pixel to pixel sensitivity variations), t is the exposure time of the image (in seconds), and $R(\lambda, T)$ is defined in (2) and in Table 1. The dark current of the camera (i.e., the signal that does not correspond to photons incident onto the detector) is insignificant at the low Martian temperatures experienced by the lander camera and is not subtracted for the calculations presented here. During Mars Pathfinder surface operations, the largest dark current of the camera (1400 hours local solar time, camera temperature −9°C) was <2 counts/s (less than 0.5% in radiance for well-exposed pixels).

3. CIE Colorimetry

The modern science of colorimetry began with *Maxwell* [1860], and in 1931 the International Commission on Illumination (Commission Internationale de l'Eclairage, or CIE) defined the formalism for quantifying color vision that is used today [*Wyszecki and Stiles*, 1982]. This system has three components (corresponding to the red, green, and blue components of human vision). The tristimulus values represent the integrated intensity of incoming radiation weighted by a set of color matching functions and are given by

$$X = K\int_0^\infty S(\lambda)\bar{x}(\lambda)\,d\lambda \tag{4a}$$

$$Y = K\int_0^\infty S(\lambda)\bar{y}(\lambda)\,d\lambda \tag{4b}$$

$$Z = K\int_0^\infty S(\lambda)\bar{z}(\lambda)\,d\lambda \tag{4c}$$

where $S(\lambda)$ is the spectral radiance of the object as a function of wavelength and $\bar{x}$, $\bar{y}$, and $\bar{z}$ are the CIE color matching functions (CMFs). The CMFs represent the amount of the three primary colors necessary to match a monochromatic stimulus and are related (but not equal) to the spectral sensitivity curves of the three types of cones in the typical human retina.

By design, $\bar{y}$ is the photopic response of the human eye over the visible wavelength region. As a consequence, the Y tristimulus value is also a measure of the luminance (relative brightness) of an object. Both the spectral reflectance of an object and the illumination conditions under which it is viewed determine the color and luminance of an object; the spectral radiance $S(\lambda)$ of an object is the product of its reflectance $r(\lambda)$ and the incident irradiance $I(\lambda)$:

$$S(\lambda) = \frac{I(\lambda)r(\lambda)}{\pi} \tag{5}$$

The normalization constant K in (4) is given by

$$K = \frac{100}{\displaystyle\int_0^\infty S_L(\lambda)\bar{y}(\lambda)\,d\lambda} \tag{6}$$

where $S_L(\lambda)$ is the radiance of a perfect Lambertian reflector ($r(\lambda) = 1$), and $I(\lambda)$ is approximated as the value of the solar flux above the atmosphere.

The chromaticities of an object (pixel) are found by normalizing the tristimulus values

$$x = X/(X + Y + Z) \tag{7a}$$

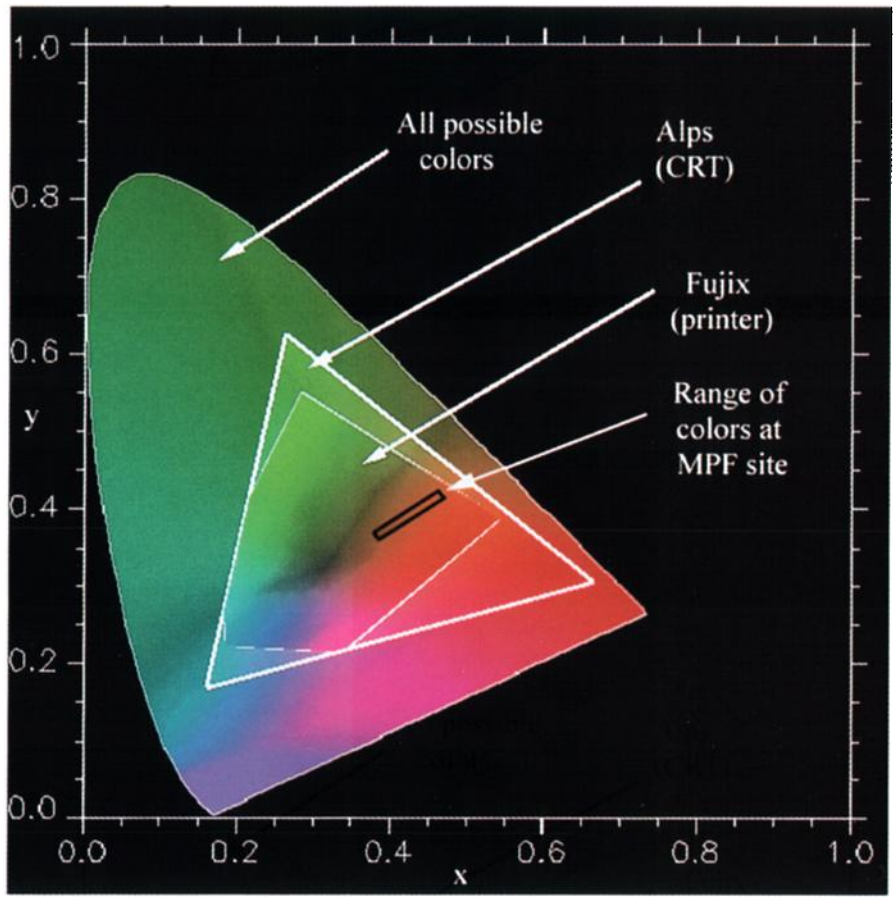

Plate 1. A CIE *xy* chromaticity diagram, containing the color coordinates of all possible colors, along with a schematic representation of the range of colors seen at the Pathfinder landing site. The curved edge of the color gamut is called the spectral locus and corresponds to the color of monochromatic stimuli. Superimposed onto the CIE color space is the gamut of a calibrated CRT computer monitor (an additive *RGB* device) named "Alps." The *R*, *G*, and *B* device primaries correspond to the vertices of the triangle. Colors within the triangle (i.e., within the gamut) are generated by combining the *RGB* primaries. Colors outside the triangle cannot be generated and must be desaturated (i.e., brought into the device gamut) before being displayed. The gamut of a hard-copy printer (in this case a subtractive *CMYK* device named "Fujix") is smaller than the gamut of the CRT monitor. For illustrative purposes the relative brightnesses of the three gamuts have been arbitarily varied.

$$y = Y/(X + Y + Z) \quad (7b)$$

$$z = Z/(X + Y + Z) \quad (7c)$$

Because $x + y + z = 1$, z is redundant. Thus the x and y chromaticities (along with the luminance Y) define a color. Plate 1 shows a chromaticity diagram containing the gamut of all possible colors. Within this gamut we show the gamut of two output devices (a CRT and a hard-copy printer), along with the range of chromaticities measured at the Pathfinder landing site.

For more detailed discussions of CIE colorimetry, see *Wyszecki and Stiles* [1982] or *Hunt* [1995].

4. Computing Tristimulus Values

There are three commonly used methods of converting from radiance units to color coordinates. We use method 1 in this paper.

4.1. Method 1

If the instrument measuring the spectrum of an object or scene has arbitrarily high spectral resolution, the radiance at each wavelength point is known exactly, and the tristimulus values can be calculated directly from the measured radiance spectrum. Because the camera samples the spectrum at discrete points, the spectrum $S(\lambda_i)$ is modeled as a curve (cubic spline) passing through each measured radiance point. $S(\lambda_i)$, in units of radiance, is integrated with the CMFs in (4) to obtain the XYZ tristimulus values, expressed below as sums:

$$X_t = K \sum S(\lambda_i)\bar{x}(\lambda_i) \quad (8a)$$

$$Y_t = K \sum S(\lambda_i)\bar{y}(\lambda_i) \quad (8b)$$

$$Z_t = K \sum S(\lambda_i)\bar{z}(\lambda_i) \quad (8c)$$

where the functions are summed discretely over the wavelength range for which $S(\lambda_i)$ is known.

Table 2. Data Used for Color Calculations

Panorama Name	Camera Sequence Numbers	Filters Used[a]	Compression Ratio	Time of Day	Sol	Notes
Gallery	0164–0166	R0 (440nm)	6:1	1100–1300 LST	9–11	entire panorama acquired during the same time of day, over a period of 3 days
		R5 (670nm)	6:1			
		R9 (530nm)	6:1			
Superpanorama	0181–0188	R0 (440nm)	lossless[b]	various; generally in the morning	13–83	acquired at various times of day; R9 and R10 overexposed in some frames.
		R10 (480nm)	2:1			
		R9 (530nm)	2:1			
		R8 (600nm)	2:1			
		R5 (670nm)	lossless			

[a]R, right eye; L, left eye.
[b]Early portions of this panorama were initially taken 2:1 JPEG in R0.

4.2. Method 2

The tristimulus values can also be calculated directly by expressing them as a linear function of the measured radiances. Using this method, the tristimulus values are related to intensity by observing a set of i targets with known spectra (tristimulus values) in each of j filters and expressing X, Y, and Z as a linear combination of the camera responses $S(i, j)$:

$$X_i = a_1 S_{i1} + a_2 S_{i2} + a_3 S_{i3} + \cdots + a_j S_{ij} \quad (9a)$$

$$Y_i = b_1 S_{i1} + b_2 S_{i2} + b_3 S_{i3} + \cdots + b_j S_{ij} \quad (9b)$$

$$Z_i = c_1 S_{i1} + c_2 S_{i2} + c_3 S_{i3} + \cdots + c_j S_{ij} \quad (9c)$$

The number of XYZ equations in (9) is equal to the number of targets measured, and the number of terms in each equation is equal to the number of filters in the camera system. The a, b, and c terms in the above equations are typically solved from the overdetermined set of XYZ equations by least squares. This method was used by the Galileo project for the solid-state imaging (SSI) instrument [*Klassen and Breneman*, 1988].

4.3. Method 3

When the filters of a camera system are broad relative to their spectral separation or have substantial out of band sensitivity, the above methods inaccurately calculate the tristimulus values. In this case the spectrum must be estimated by modeling it as a sum of basis functions. This requires detailed knowledge of the camera response as a function of wavelength, and the observed spectrum is determined by iteratively integrating it with the camera response function until the observed camera signal DN is obtained. This method was used for the Viking cameras [*Park and Huck*, 1976; *Huck et al.*, 1977]. Method 1 was then used to obtain the tristimulus values.

4.4. Chromaticity Analysis

We used several sets of image data for our analysis. The first set is from the "gallery panorama," a three-filter panorama acquired around local noon. Images in this panorama were compressed at 6:1 using the modified IMP Joint Photographic Experts Group (JPEG) compressor [*Smith et al.*, 1997]. This time-continuous panorama contains over 10 million individual pixels per filter and covers the entire landing site. The second data set used in our analysis is a five-filter subset of the "superpanorama," a multispectral panorama compressed losslessly in two filters and JPEG-compressed at 2:1 in all other geology filters (over 6 million individual pixels per filter). Unlike the gallery pan, the superpan is not time continuous from frame to frame and does not cover the entire surface. Although the JPEG compression artifacts add noise to the measurements, we find that the computed color parameters are not significantly affected by lossy (6:1) compressed data (compared to the calculated color parameters from losslessly compressed data). For a more detailed discussion of the effects of JPEG compression on IMP images, see *Reid et al.* [this issue]. Table 2 summarizes the two data sets. We note that color estimates from the five-filter data have x chromaticities which are 0.01 higher than the three-filter data, and the five-filter data have y values slightly less (0.005) than the three-filter data. This difference is at the limit of human perceptibility [*Wyszecki and Stiles*, 1982]. We list the five-filter chromaticity values in Table 3.

Figure 1 shows two individual images of the Pathfinder landing site from the data set listed in Table 2. The images contain the five major color groups of material at the landing site: unshadowed soil, shadowed soil, rocks, a rock/soil mix, and the sky. See Figure 2 for the absolute spectral radiance of the soil, rock, and sky. Scatterplot chromaticity diagrams of these images (Figure 3) show that the color distribution on the surface is continuous and occupies a relatively small region in the CIE colorspace (i.e., the color variation is relatively small). In Figure 3, we have indicated the approximate boundaries of the color classes in the CIE colorspace. Though the boundaries are not distinct, the classes of material can be seen in the scatterplots. Figure 3b shows the sky as a distinct object. Below, we present techniques for redefining the colorspace to enhance these color differences.

The Inter-Society Color Council–National Bureau of Standards (ISCC–NBS) defined a standard color naming convention which defines color names in terms of calibrated color patches [*Kelly*, 1976]. This naming convention uses a set of hue names (red, orange, yellow, green, etc.) and their adjectival forms (reddish orange, yellowish green, etc.) along with modifiers (light, dark, pale, etc.). This system was used by *Huck et al.* [1977] to describe their results, and we find them equally useful. Translation of these color names into Munsell coordinates is described by *Kelly* [1976].

The measured chromaticity (x = 0.43–0.46, y = 0.38–0.40) of the soil at the Pathfinder landing site corresponds to a moderate yellowish brown color (ISCC–NBS 77) and is in agreement with the Viking values (Table 3). The color of the surface as a function of azimuthal look angle does not signif-

Plate 2. The true color of Mars based upon three filters with the sky set to a luminance of 60. The color of the Pathfinder landing site is yellowish brown with only subtle variations. These colors are identical to the measured colors of the Viking landing sites reported by *Huck et al.* [1977]. This image should be illuminated with direct sunlight (or the corresponding CIE D65 illuminant) and viewed without surroundings containing brilliant colors.

Plate 3. Color enhancement resulting from a multiplication of the saturation of the image in Plate 2 by a factor of 3. Hue and luminance have been largely preserved. Indistinct colors become artificially more vivid without a major loss of color balance.

Plate 4. Color enhancement of Plate 2, resulting from the movement of the chromaticity coordinate $x = 0.405$ and $y = 0.380$ to neutral gray followed by a multiplication of the saturation by 3. Colors are now distributed about a new coordinate origin corresponding to the center of the distribution. With this artificial mapping, the eye can now easily discriminate between the colors of rocks, soil, and sky.

Plate 5. Color enhancement resulting from moving the chromaticity coordinate $x = 0.405$ and $y = 0.380$ to neutral gray, multiplying the saturation by 5, and replacing the luminance image by a constant of $Y = 25$. This eliminates the brightness variation in the image and enhances color differences. The colors of the shadows are now visible. Shadows are the reddest features, and the sky can be seen to more closely resemble the hue of rocks rather than soil.

Table 3. Color Estimates of the Martian Sky and Surface From Pathfinder (this paper) and Viking [*Huck et al.*, 1977]

Location	Pathfinder		Viking 1		Viking 2		ISCC–NBS Color Designation
	x	*y*	*x*	*y*	*x*	*y*	
Sky	0.39–0.41	0.37–0.38	0.40	0.38	0.40	0.38	76–77 (light to moderate yellowish brown)
Rock	0.38–0.41	0.35–0.39	...	...	...	...	81 (dark grayish yellowish brown)
Rock/soil	0.41–0.43	0.38–0.40	...	...	...	...	58 (moderate brown)
Soil	0.43–0.45	0.38–0.41	0.43–0.46	0.39–0.40	0.43–0.44	0.39	77 (moderate yellowish brown); 78 (dark yellowish brown); 58 (moderate brown)
Shadowed soil	0.45–0.47	0.39–0.41	0.46	0.39	0.44	0.39	59 (dark brown)
Pathfinder Rover tracks	0.44	0.39	...	...	...	...	58 (moderate brown)

Data show the color of the sky and soil to be identical to the Viking sites. We compared (visually, with a color meter, and with the Color Names Dictionary [*Kelly*, 1976]) our prints to the ISCC–NBS centroid color chips [*Kelly and Judd*, 1968]. We find the sky color to be closest to ISCC–NBS chip 76 (light yellowish brown) and the soil color to chips 77 (moderate yellowish brown), 78 (dark yellowish brown), and 58 (moderate brown). Our matches to the ISCC–NBS color chips agree with those listed by *Huck et al.* [1977]. Additionally, we find the shadowed soil color as ISCC–NBS chip 59 (dark brown), and the color of the rocks as ISCC–NBS chip 81 (dark grayish yellowish brown).

icantly change (Figures 4 and Plate 2). We also note that the soil color is independent of time of day.

The light to moderate yellowish brown color (x = 0.395–0.405 and y = 0.370–0.380, or ISCC–NBS colors 76 and 77) of the noontime sky near the horizon is consistent with the sky color seen at the Viking sites [*Huck et al.*, 1977]. The sky color varies as a function of time of day and azimuthal look angle (Figure 5). Figure 5 also shows that the sky is slightly redder in the anti-Sun direction and bluer in the direction of the Sun. This relative change in color is at the limit of perceptibility and would probably be difficult to notice with the naked eye while standing on the Martian surface. Figure 6 shows the color of the sky as a function of elevation, indicating that the sky reddens slightly near the horizon.

The color of the rocks at the Viking site was not reported due to difficulties in obtaining reproducible measurements [*Huck et al.*, 1977]. We include the color of the Pathfinder rocks here and note that the rock radiance spectra are essentially identical in shape to the sky spectra except for a uniform intensity scale factor (where the sky is approximately 3 times brighter than the soil; see Figure 2). Thus the rock color (x = 0.38–0.42, y = 0.35–0.39) is similar to the sky color, and the perceived color difference between the sky and the rocks is due to the difference in brightness. The luminance values of the rocks are low enough that the rock color appears visually as gray, and if the brightness of the scene is set to be uniform throughout, the rocks and the sky have the same perceived color (Plate 5).

The color of the sky at sunrise and sunset is considerably different from the color of the noontime sky near the horizon. The sunrise/sunset sky has average chromaticity values ranging from x = 0.34 to 0.36 and y = 0.34 to 0.36, which correspond to a grayish olive color (ISCC–NBS 110) or a brownish gray color (ISCC–NBS 64). This sky color becomes bluer toward the Sun, transitioning gradually from brownish gray at 15° to a bluish white color (ISCC–NBS 189) 5° from the Sun. At 2° from the Sun the x and y chromaticities are 0.28 and 0.29 respectively, which correspond to a very pale blue color (ISCC–NBS 184) or a very light blue (ISCC–NBS 180). Figures 7–9 illustrate this effect along with Plates 6 and 7.

We also examined the color of the tracks made by the Pathfinder rover [*Rover Team*, 1997]. The color of the subsurface

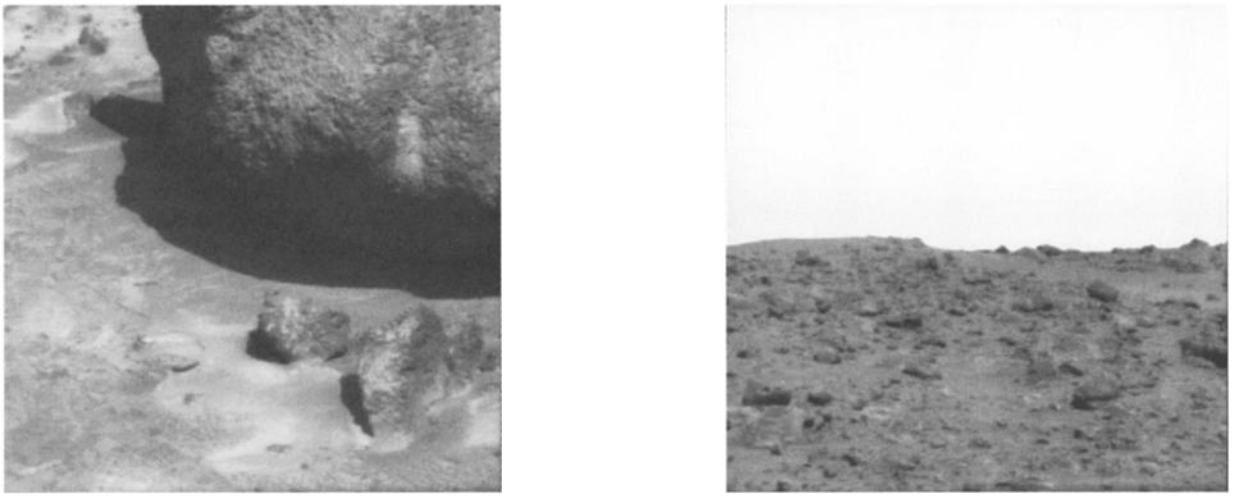

(a) (b)

Figure 1. (a) Image taken at 0937 LST on sol 66 (sol = 1 Martian day = 24.6 hours), looking to the northwest. The rock named "Yogi" is in the upper right of the image. (b) Image taken at 1100 LST on sol 10, looking north.

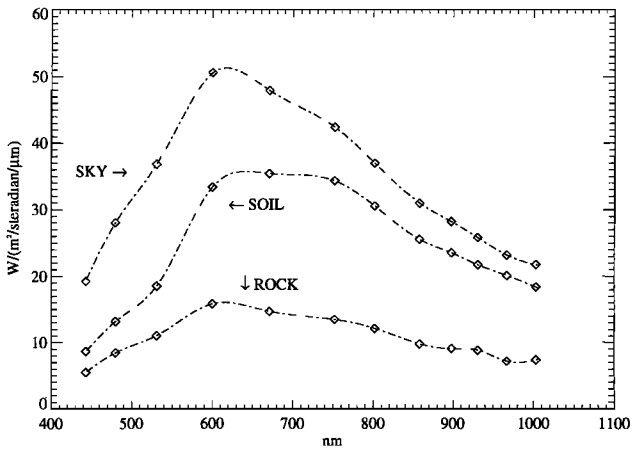

Figure 2. Spectral radiance of soil, sky, and a rock at the Pathfinder landing site. The measured data are shown as points connected with a cubic spline function. The rock spectrum and the sky spectrum have similar shapes, differing only by a constant scale factor in intensity (the scale factor for this particular example is approximately 3.2). The soil spectrum has a distinctly different shape than the sky or the rock spectra.

soil in the tracks ($x = 0.44$ and $y = 0.39$) is identical to the color of the surface soil material. A similar result was also reported by *Huck et al.* [1977] with the Viking trench soil.

5. Displaying the Color Data on Output Devices

Calculation of the CIE tristimulus values is a well-defined mathematical operation, and manipulation of these values (in the CIE colorspace) is a relatively straightforward process. Displaying the colors on output devices, however, is nontrivial and requires a careful calibration of the particular device. The xyY units calculated from (4) and (7) are in the CIE colorspace and are device independent. The image DN values of R, G, and B need to be specified through an xyY calibration table for a specific device. Similarly, radiance values must first be transformed through (4) into colorimetric units before being transformed into device units.

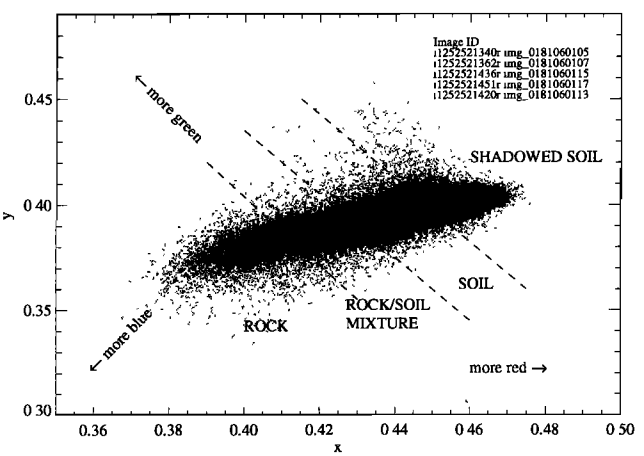

Figure 3a. Chromaticity plot for the image shown in Figure 1a. The values of x and y correspond to a yellowish brown color. The relative "redness" of the material increases from left to right. These data were computed using five filters.

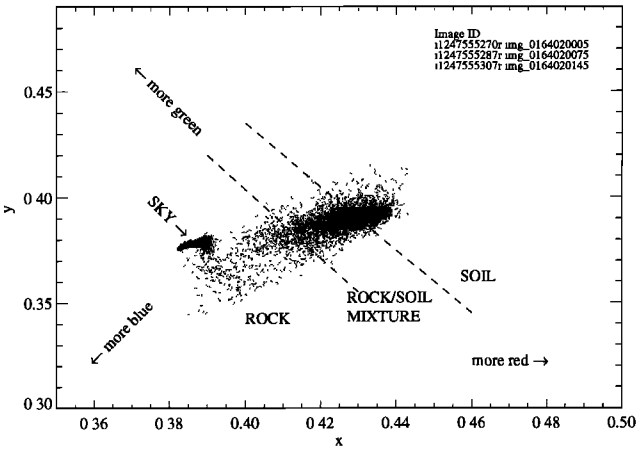

Figure 3b. Chromaticity plot for the image shown in Figure 1b. Only a representative portion of the pixels is shown in order to highlight the sky cluster. The sky chromaticity is within the range of values measured for the rocks. These data were computed using three filters.

5.1. Output Device Calibration

At the Jet Propulsion Laboratory (JPL) Multimission Image Processing Laboratory (MIPL) we calibrate our devices by measuring the xyY output for a large number of combinations of RGB input intensities and then interpolate to determine the amount of each device primary required to reproduce the desired xyY output values. This is done by displaying a data cube containing combinations of pixel RGB values onto the device and measuring the resulting xyY colorimetric response photometrically for each combination of RGB values. The cube typically contains 1000 xyY values (10 by 10 by 10). To calibrate a computer monitor, we strap a color meter onto the screen and measure these xyY values directly. The chromaticities of hard-copy prints are measured with a meter under a known illuminant such as D65 (Earth daylight, cloudless sky) using the same xyY cube approach.

Once the xyY cube has been populated for a particular device, the neighborhood of any target xyY value can be located and the corresponding RGB value interpolated within the xyY space. The xyY space is nonlinear in terms of equal

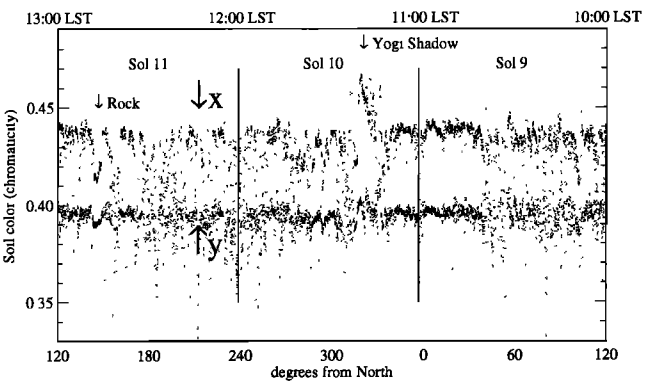

Figure 4. A 360°, 1-pixel-high strip of the surface color as a function of azimuthal look angle, showing that the average chromaticity does not vary as a function of azimuth. Note the relative redness of the "Yogi" rock shadow relative to the relative blueness of the rock material. See Plate 2 for the corresponding color print.

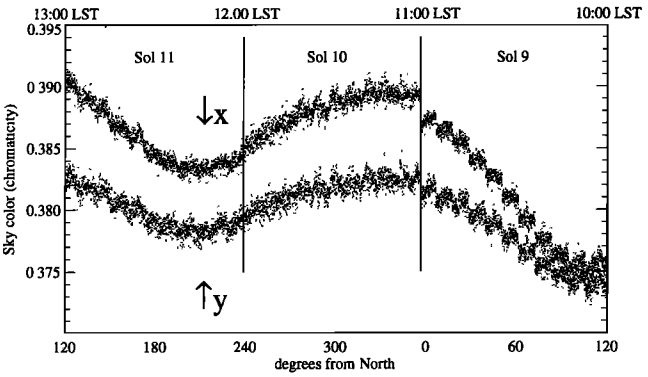

Figure 5. A 360°, 1-pixel-high strip of the chromaticity of the Martian sky as a function of both azimuthal look angle and local time, showing that the Martian sky color varies azimuthally and temporally. The data shown are from the three-filter "gallery panorama." The panorama was acquired in a time-continuous fashion over a span of 3 days (from right to left in the figure). Local Mars time is on the top x axis and increases from right to left. The sky reddens slightly when looking toward the anti-Sun direction (north). The sky also reddens slightly from 1000 to 1100 LST. The "staircase" effect (most evident on sol 9) is due to 5 min pauses (during which the surface was being imaged) between the sky images. The large "step" between sol 9 and 10 is due to a 20 min difference in local acquisition time. See Plate 2 for the corresponding color print.

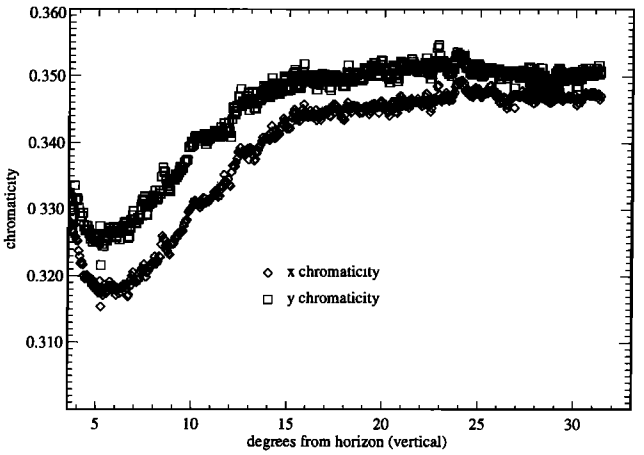

Figure 7. Sunrise, sol 39. The sky color at sunrise shows the same grayish brown color as seen at sunset. These predawn data show a reddening of the sky very near the horizon (<5° elevation), similar to the reddening shown in Figure 6. See Plate 6 for the corresponding color print.

perceptual differences and is actually converted to a linear photovisual space such as $L^*a^*b^*$ or $L^*u^*v^*$ before the lookup process. In this fashion, any device can be modeled, whether it is additive (television monitor) or subtractive (film recorder or printer). The problem would be straightforward if all devices could reproduce all colors, but unfortunately, the gamut of any device is limited to a region between the chromaticities of its primaries in the xy chromaticity plane (Plate 1). This region narrows at low and high luminance. The problem of how to reassign out-of-gamut colors to others within the gamut of the device while preserving the hue is topologically complex, and we use the Candela commercial package offered by Candela, Ltd. of Burnsville, Minnesota, for mapping colors between devices.

5.2. Color Prints

The hard-copy prints in this paper must be viewed under the D65 illuminant (equivalent to Earth daylight on a clear day) in order to reproduce the correct color. We find that while artificial lighting (generally fluorescent) seems to produce acceptable results, viewing the prints under Earth sunlight on a clear day optimizes the color reproduction.

Using the techniques described above, we created color panoramas of the Pathfinder site using the three-filter "gallery" panorama data. Figure 10 shows the x and y chromaticity values of the landing site as grayscale images. Plate 2 shows a color image of Mars as it would be seen by a human observer on the Martian surface. Nearly everything is a similar yellow

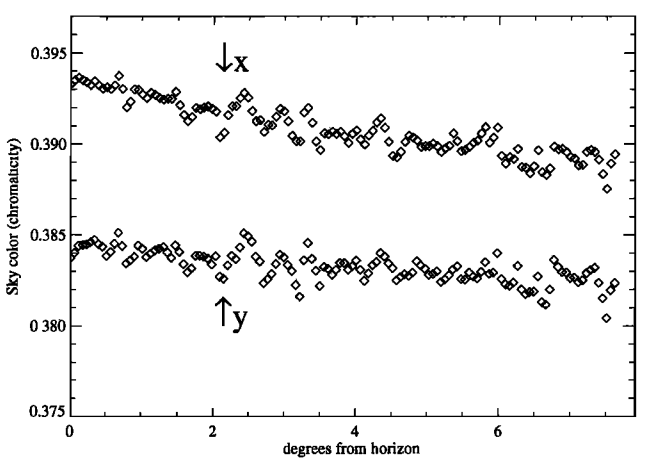

Figure 6. Sky color versus elevation, 1115 LST, NW direction. The sky is slightly redder near the horizon. See Plate 2 for the corresponding color print.

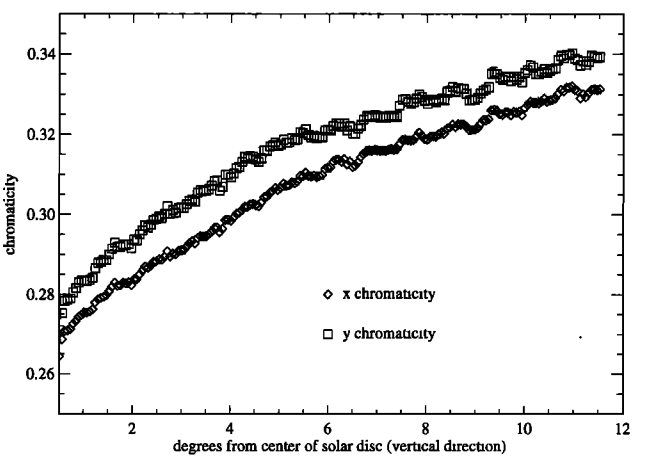

Figure 8. Sunset, sol 24. The color of the sky at sunset, shown as a function of vertical elevation. The sky slowly reddens away from the Sun, in the vertical direction. The color of the sky near (within 2°) the Sun is a very pale blue (ISCC–NBS 184), and farther away from the Sun (15°) the sky is a brownish gray color (ISCC–NBS 64), with a slight hint of a grayish moderate olive brown (ISCC–NBS 95). See Plate 7 for the corresponding color print.

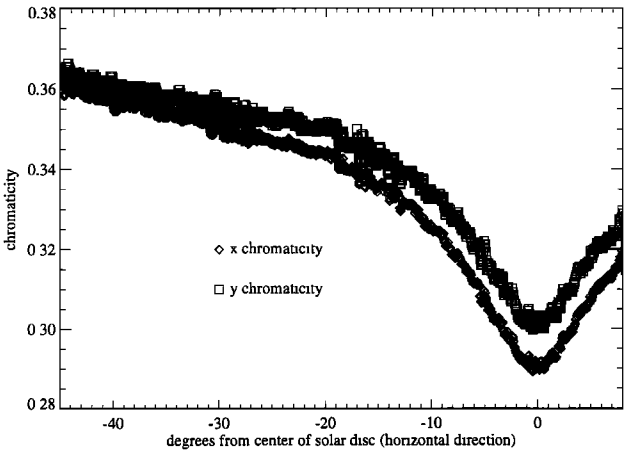

Figure 9. Sunset, sol 24. The color of the sky at sunset, shown as a function of azimuth. The sky becomes bluer toward the Sun. At −40° the sky is a brownish gray color (ISCC–NBS 64) to grayish olive (ISCC–NBS 110). See Plate 7 for the corresponding color print.

brown color, and the surface color is independent of the azimuthal look angle. Variations in the sky are apparent, with a reddening away from the Sun and toward the horizon. We have verified the chromaticities of the image in Plate 2 by measuring the print with a calibrated color meter and are working with the publisher to ensure correct color reproduction of the print.

6. Color Enhancements

The images in Plates 3–5 are color enhancements of the image in Plate 2. Up to this point, we have discussed a method for reproducing the color of a scene such that a viewer would experience the same color sensation viewing the displayed image as he or she would have if present at the scene. The value of true color is twofold: one, that a person can vicariously identify with a scene and, two, that they can apply their experience in interpreting colors to interpret the image. But because the eye must deal with a broad range of possible spectra, it cannot discriminate well between similar colors, such as those on Mars. We can however, manipulate the data in order to mimic an eye with greater discriminability. To do so, we take advantage of a color coordinate system called $L^*u^*v^*$, in which the separation between points is roughly equal in perception [*Wyszecki and Stiles*, 1982]. L^*, u^*, and v^* are defined as

$$L^* = 116(Y/Y_0)^{1/3} - 16 \tag{10a}$$

$$u^* = 13L^*(u - u_0) \tag{10b}$$

$$v^* = 13L^*(v - v_0) \tag{10c}$$

where

$$u = \frac{4X}{(X + 15Y + 3Z)} \tag{11a}$$

$$u_0 = \frac{4X_0}{(X_0 + 15Y_0 + 3Z_0)} \tag{11b}$$

$$v = \frac{9Y}{(X + 15Y + 3Z)} \tag{11c}$$

$$v_0 = \frac{9Y_0}{(X_0 + 15Y_0 + 3Z_0)} \tag{11d}$$

and X_0, Y_0, and Z_0 refer to the tristimulus values of a reference white such as D65. The $L^*u^*v^*$ system has the additional property that hue H_{uv} and saturation S_{uv} can be defined as

$$H_{uv} = \tan^{-1}\left(\frac{v^*}{u^*}\right) \tag{12}$$

$$S_{uv} = \frac{[(u^*)^2 + (v^*)^2]^{1/2}}{L^*} \tag{13}$$

where hue is the attribute of color which is generally assigned as red, yellow, or green, saturation is the degree to which a color differs from a monochromatic stimulus independent of the luminance of the object, and L^* is a measure of luminance more equitably distributed in perception. The distribution of colors from a Mars surface image in the $L^*u^*v^*$ space tends to cluster in such a way that much of the color space is empty. To better discriminate colors, we expand the information uniformly in the space while remaining in the device gamut. We have found three transformations to be most useful.

The first transformation converts xyY imagery into L^*, S_{uv}, H_{uv} followed by a subsequent multiplication of S_{uv} by a number greater than unity. This increases the saturation of the scene, moving it toward the edge of the device gamut. We then transform back to *RGB* using the device calibration. Plate 3 illustrates this technique. In this case the effective sensitivity of the eye (to saturation) is increased by a factor of 3. Nearly all the colors cluster in the same direction.

The second transformation converts xyY imagery into L^*, S_{uv}, H_{uv} followed by a translation of the u^*, v^* point of $x = 0.4050$, $y = 0.3800$ to the gray origin at $u^* = 0$, $v^* = 0$. We then multiply the saturation by 3.0 before converting back to RGB. Plate 4 illustrates the effect. The coordinate shift corresponds to a point in xy space midway between rocks and soil. The result is a map in which the eye can easily discriminate between these classes. This transformation maintains order in the color space at the sacrifice of losing the hue information.

The third transformation is similar to that of Plate 4 except the saturation has been multiplied by 5 and the luminance has been discarded and replaced by a constant of 25. This transformation eliminates intensity variations. All colors can now be seen, even within shadows. Shadowed surfaces are the reddest of any feature, and the sky color resembles more the rocks than the soil (Plate 5).

Plate 6 is a true color, six-frame mosaic of the pre-sunrise sky, illustrating the variation in color away from the Sun. The same effect occurs at sunset (Plate 7a). Because the natural scene has such low saturation, the eye has trouble discriminating colors. To improve discriminability, the image saturation in Plate 7a was multiplied by 2 and is shown in Plate 7b. Here one can readily perceive the shift away from blue toward the daylight hues of the sky seen away from the Sun.

7. Conclusions

The color of the Pathfinder landing site is yellowish brown with subtle variation; our measured chromaticity values for the surface agree with the values at the Viking sites [*Huck et al.*, 1977]. The color of the terrain is independent of time of day. We also observe that the sky reddens away from the Sun, toward the horizon, and is reddest at local noon. Sunrise and

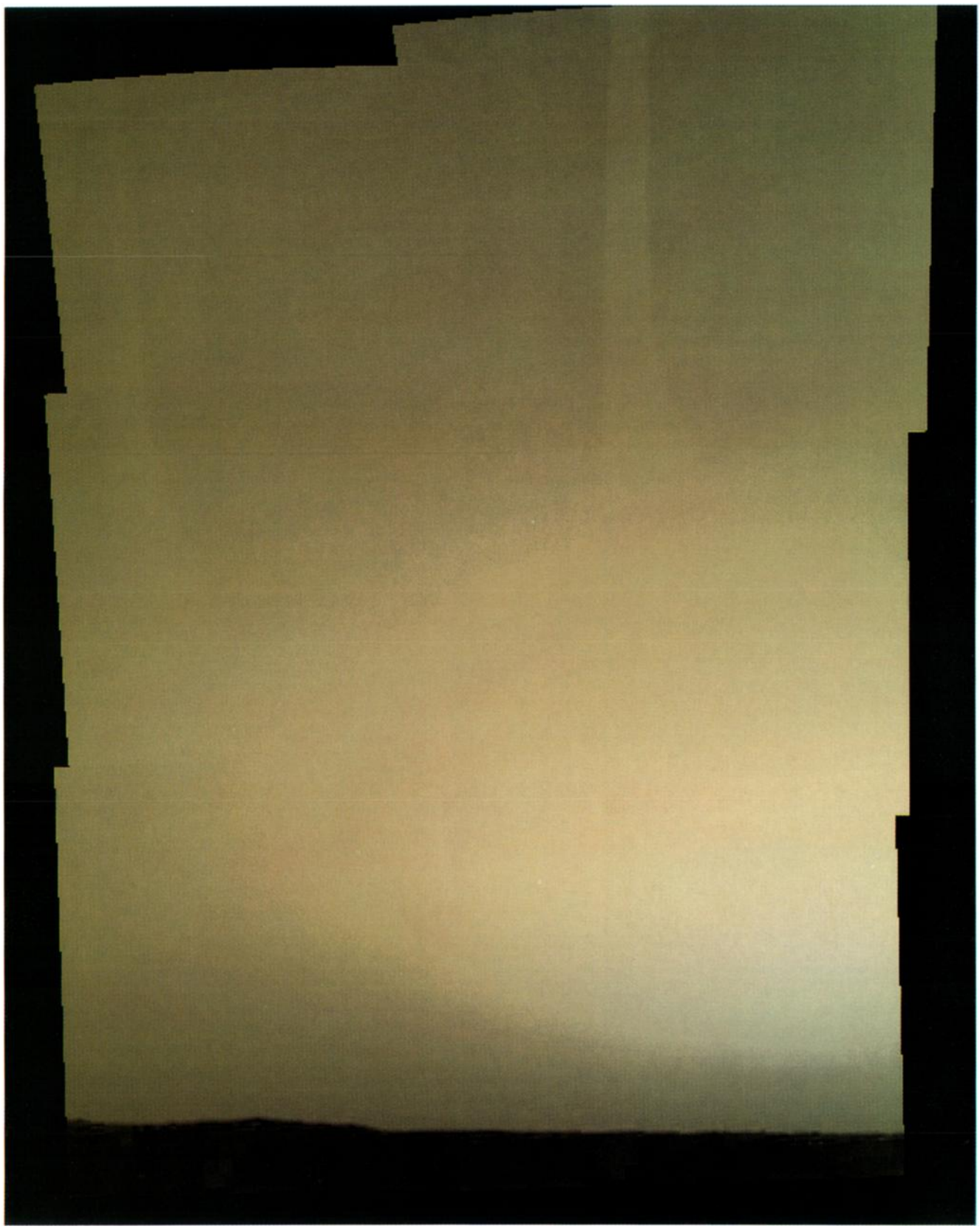

Plate 6. Sunrise, sol 39. This true color, pre-sunrise image (approximately 0530 LST) is composed of six images extending 30° in azimuth and 45° in elevation and shows the brownish gray predawn sky.

Plate 7a. The brownish gray sky as it would be seen by an observer on Mars in this four-frame, true color mosaic taken on sol 24 (at approximately 1610 LST). The twin peaks can be seen on the horizon. The sky near the Sun is a pale blue color. Azimuth extent is 60°, and elevation extent is approximately 12°.

Plate 7b. Color-enhanced version of the image in Plate 7a, produced by multiplying the saturation by 2. Colors which were previously gray now become more apparent.

Figure 10a. The x chromaticity of the Pathfinder landing site, shown as a grayscale image. The grayscale intensity is roughly proportional to the redness of the scene.

Figure 10b. The y chromaticity of the Pathfinder landing site, shown as a grayscale image. Because the variation in y is at a smaller level than the x variation and thus scaled differently, the image appears noisier than the image in Figure 10a.

sunset images reveal a grayish brown color, with the sky becoming blue toward the Sun. The color enhancement techniques presented here allow the images to be manipulated to reveal subtle relative color differences while retaining color balance.

Acknowledgments. We acknowledge the dedication and hard work of the entire Mars Pathfinder team. We thank K. Herkenhoff for thoughtful reviews of this manuscript. A. Runkle, D. Alexander, K. Capraro, M. McAuley, E. Duxbury, P. Woncik, S. Suzuki, E. DeJong, S. LaVoie, T. Handley, B. Green, and many others contributed to the success of Pathfinder image processing during the operational phase of the mission. We thank the JPL photographic laboratory for the use of a color meter to measure the color prints presented in this paper. Work described in this paper was carried out by the Mars Pathfinder Project at the Jet Propulsion Laboratory, California Institute of Technology, under contract with the National Aeronautics and Space Administration.

References

Huck, F. O., D. J. Jobson, S. K. Park, S. D. Wall, R. E. Arvidson, W. R. Patterson, and W. D. Benton, Spectrophotometric and color estimates of the Viking lander sites, *J. Geophys. Res.*, *82*(28), 4401–4411, 1977.

Hunt, R. W. G., *Measuring Colour*, 2nd ed., Ellis Horwood, Chichester, England, 1995.

Kelly, K. L., Color: Universal language and dictionary of names, *NBS Spec. Publ. 440*, U.S. Dep. of Commer., Natl. Bur. of Stand., Gaithersburg, Md., Dec. 1976.

Kelly, K. L., and D. B. Judd, ISCC-NBS centroid color system, in *Manual of Color Aerial Photography*, 1st ed., edited by J. T. Smith, p. 523, Am. Soc. of Photogramm., Falls Church, Va., 1968.

Klaasen, K., and H. Breneman, Galileo solid state imaging subsystem calibration report: Part 1, *JPL Internal Doc. D-5880*, pp. 177–186, Jet Propul. Lab., Pasadena, Calif., Nov. 1, 1988.

Maxwell, J. C., On the theory of compound colours and the relations of the colours of the spectrum, *Proc. R. Soc. London*, *10*, 1860.

Park, S. K., and F. O. Huck, A spectral reflectance estimation technique using multispectral data from the Viking lander camera, *NASA Tech. Note*, *D-8292*, 1976.

Reid, R. J., et al., IMP image calibration, *J. Geophys. Res.*, this issue.

Rover Team, Characterization of the Martian surface deposits by the Mars Pathfinder rover, Sojourner, *Science*, *278*, 1765–1768, 1997.

Smith, P. H., et al., The Imager for Mars Pathfinder, *J. Geophys. Res.*, *102*(E2), 4003–4025, 1997.

Wyszecki, G., and W. S. Stiles, *Color Science: Concepts and Methods, Quantitative Data and Formulae*, 2nd ed., John Wiley, New York, 1982.

R. D. Brandt, J. J. Lorre, J. N. Maki, and D. J. Steinwand, Jet Propulsion Laboratory, California Institute of Technology, MS 168-414, 4800 Oak Grove Drive, Pasadena, CA 91109. (e-mail: justin.maki@jpl.nasa.gov)

P. H. Smith, Lunar and Planetary Laboratory, University of Arizona, Tucson, AZ 85721.

(Received February 3, 1998; revised May 20, 1998;
accepted May 26, 1998.)